

## Direct photon and neutral pion production in pp and Pb–Pb collisions measured with the ALICE experiment at LHC

D. Peressounko\* for the ALICE Collaboration

*RRC "Kurchatov institute",  
Kurchatov sq.,1, Moscow, 123182, Russia  
\*E-mail: Dmitri.Peressounko@cern.ch*

Measurements of direct photon and neutral pion production in heavy-ion collisions provide a comprehensive set of observables characterizing properties of the hot QCD medium. Direct photons provide means to test the initial stage of an AA collision and carry information about the temperature and space-time evolution of the hot medium. Neutral pion suppression probes the parton energy loss in the hot medium. Measurements of neutral meson spectra in pp collisions at LHC energies  $\sqrt{s} = 0.9, 2.76, 7$  TeV serve as a reference for heavy-ion collisions and also provide valuable input data for parameterization of the QCD parton Fragmentation Functions. In this talk, results from the ALICE experiment on direct photon and neutral pion production in pp and Pb–Pb collisions are summarized.

*Keywords:* Direct photons; neutral pions; quark-gluon matter.

### 1. Introduction

The ultimate goal of heavy ion collisions is a detailed study of the properties of quark-gluon matter. Photons provide tools for testing almost all key features of this hot matter: spectra and correlations of hard hadrons, which can be reconstructed using photon decays, test the energy loss of energetic partons in hot matter and the collective flow of identified hadrons up to high  $p_T$ . *Direct* photons, defined as photons not from hadronic decays, are made up of *prompt* photons (emitted by partons of colliding nucleons) and *thermal* photons (emitted by the hot matter analogously to blackbody radiation). The former allows us to probe the initial state of the collision while the latter reflects the temperature and the space-time evolution of the matter. In addition, the thermal-photon flow reflects the development of the hot matter's collective flow at all stages of the collision.

### 2. Experimental Setup

A detailed description of the ALICE experimental setup can be found in<sup>1</sup>. Compared to other LHC experiments, ALICE excels at low- $p_T$  physics and advanced particle identification. The core of ALICE is the central tracking system consisting of the Inner Tracking System and the Time Projection Chamber. Charged particle identification is improved by the Transition Radiation Detector and Time Of Flight detector. Finally, ALICE has two calorimeters, the PHoton Spectrometer (PHOS)

2

and the electromagnetic calorimeter (EMCal), as well as a set of smaller detectors for triggering and characterizing events.

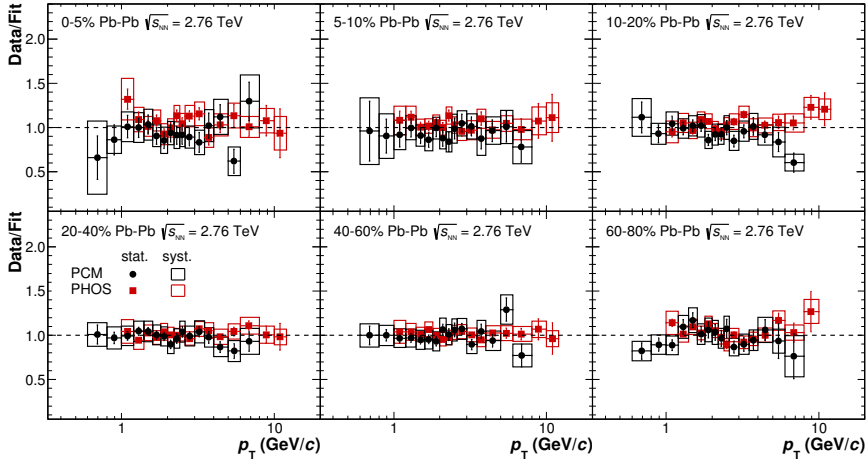


Fig. 1. Comparison of  $\pi^0$  spectra measured in Pb-Pb collisions at  $\sqrt{s_{NN}} = 2.76$  TeV in 6 centrality bins with PHOS and PCM techniques. Both spectra are divided by the fit to the combined spectrum<sup>2</sup>.

### 3. Neutral Pion Measurements

Photons can be reconstructed in ALICE in several ways: using traditional calorimetry with the PHOS and EMCal or by the Photon Conversion Method (PCM) via reconstructing  $e^+e^-$  tracks from photons conversion in the central tracking system<sup>3</sup>. PHOS has fine granularity leading to excellent energy and position resolution though it has a relatively small acceptance. PCM provides good position and energy resolution and full  $2\pi$  coverage in the azimuth. However, since ALICE was constructed to minimize the material budget, the photon conversion probability before the middle of the TPC, where tracks still can be reconstructed with high efficiency, is about 8%. As a result, both methods have comparable acceptance  $\times$  efficiencies.

The ability to simultaneously measure photon and neutral pion spectra with several independent detectors improves the reliability of the final results. Moreover, the PCM and PHOS measurements have distinct systematic uncertainties, opposite dependencies of  $p_T$  resolution and different sensitivities to pileup. The agreement between the two measurements is shown in fig. 1, where the  $\pi^0$  spectra in different centrality bins in Pb-Pb collisions at  $\sqrt{s_{NN}} = 2.76$  TeV are compared. To elucidate the comparison both spectra are divided by the fit to the combined spectrum. Within the statistical and systematic uncertainties the measurements are in good agreement<sup>2</sup>.

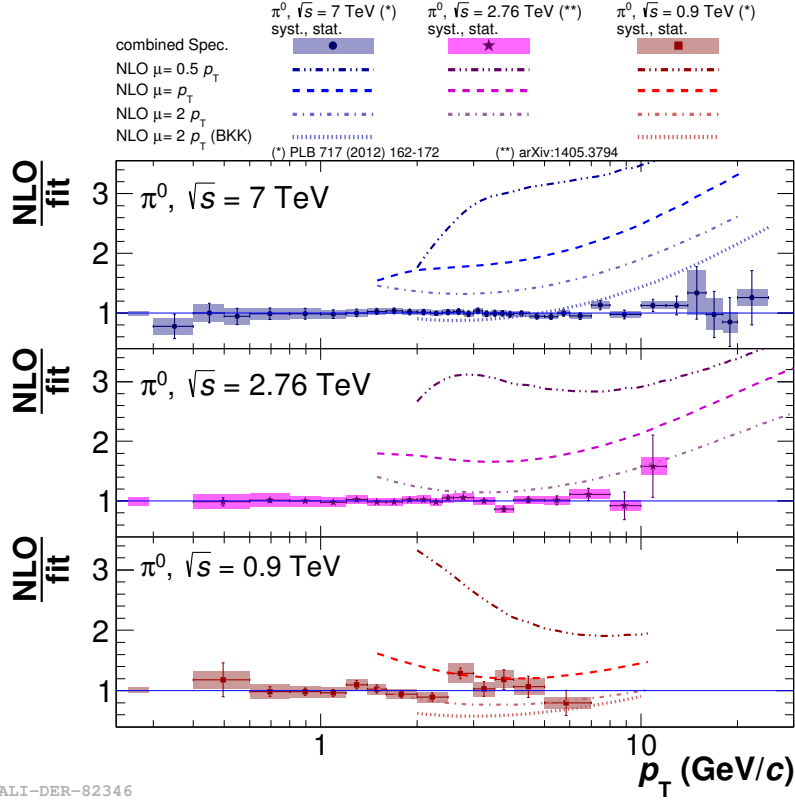


Fig. 2. Comparison of  $\pi^0$  spectra measured in pp collisions at  $\sqrt{s} = 0.9, 2.76$  and 7 TeV with several pQCD predictions. For clarity both data and predictions are divided by the fit to data.

We compare the  $\pi^0$  spectrum in pp collisions at  $\sqrt{s} = 0.9, 2.76$  and 7 TeV with several selected pQCD predictions in fig. 2. To make the comparison of steeply falling spectra clear, we fit our spectra to a function and plot ratios of the measured spectra to the fit along with the pQCD predictions to the fit<sup>3</sup>. pQCD approximately reproduces the hadron yield at the lowest LHC energy ( $\sqrt{s} = 0.9$  TeV) but overpredicts the yield by a factor of two at higher energies ( $\sqrt{s} = 2.76, 7$  TeV). This is typical for LHC measurements<sup>4</sup>. In contrast, pQCD well reproduces jet spectra in pp collisions at LHC energies<sup>5</sup>. A possible explanation is that gluon fragmentation becomes increasingly important, while the gluon fragmentation functions are not well restricted by existing data at lower  $\sqrt{s}$ . This uncertainty should be reduced in the recent calculation of fragmentation functions<sup>6</sup>, which includes these ALICE results in their global analysis.

ALICE measured neutral pion production in Pb-Pb collisions at  $\sqrt{s_{NN}} = 2.76$  TeV with two techniques: PHOS and PCM. Combined spectra were produced for 6 centrality classes. For a quantitative estimate of the parton

4

energy loss, the nuclear modification factor

$$R_{AA}(p_T) = \frac{d^2N/dp_T dy|_{AA}}{\langle T_{AA} \rangle \times d^2\sigma/dp_T dy|_{pp}} \quad (1)$$

was calculated, where the nuclear overlap function  $\langle T_{AA} \rangle$  is related to the average number of inelastic nucleon-nucleon collisions  $\langle N_{\text{coll}} \rangle$  and the pp inelastic cross section  $\sigma_{\text{inel}}^{\text{pp}}$  as  $\langle T_{AA} \rangle = \langle N_{\text{coll}} \rangle / \sigma_{\text{inel}}^{\text{pp}}$ . The neutral pion nuclear modification factors for 6 centrality bins are shown in fig. 3. At  $p_T \gtrsim 5$  GeV/c pions from hard interactions dominate and the strong suppression in  $R_{AA}$  reflects considerable energy loss for hard partons. At low  $p_T$  ( $\lesssim 2$  GeV/c) the spectrum is defined by collective (hydrodynamic) expansion and comparing with pp is not particularly meaningful. The intermediate  $p_T$  region transitions between these two regimes. In the most central collisions  $R_{AA}$  reaches a minimum of  $\sim 0.1$  indicating twice stronger suppression compared to central Au-Au collisions at RHIC energies<sup>7</sup>. Since the spectra of initial partons at LHC energies is considerably harder, stronger suppression means much larger energy loss compared to RHIC.

Fig. 3 compares the measured nuclear modification factors with predictions from two advanced models. Currently, there is no consensus as to which features are most important and should be incorporated in descriptions of energy loss in AA collisions. In the Vitev et al. model<sup>8,9</sup>, in addition to collisional energy loss, initial state effects are included, while Horowitz et al.<sup>10</sup> account for geometrical fluctuations of hard processes. Basically, both models are close to data, though Horowitz's is not as good in reproducing the centrality dependence.

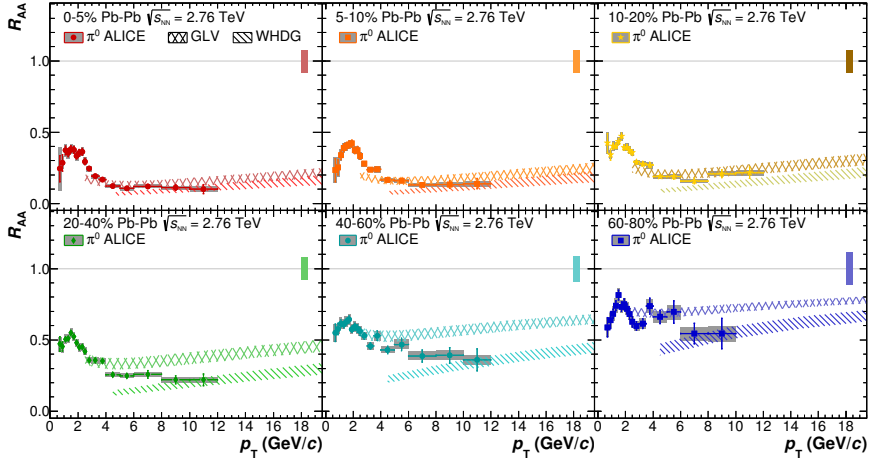


Fig. 3. Neutral pion nuclear modification factor in Pb-Pb collisions at  $\sqrt{s_{NN}} = 2.76$  GeV in 6 centrality classes<sup>2</sup>. For comparison, predictions of models of Vitev (GLV)<sup>8,9</sup> and Horowitz (WHDG)<sup>10</sup> are shown.

#### 4. Direct photon spectra and flow

ALICE measures the direct photon yield via a statistical approach; the estimated decay photon spectrum is subtracted from the measured inclusive photon spectrum. In this analysis one first constructs a double ratio

$$R_\gamma = \frac{\gamma^{inclusive} / \pi_{measured}^0}{\gamma^{decay} / \pi_{param}^0} \approx \frac{\gamma^{inclusive}}{\gamma^{decay}}. \quad (2)$$

A double ratio of unity,  $R_\gamma = 1$ , represents no direct photon yield whereas an increase above unity constitutes a presence of direct photons. The advantage of this approach is that most of the largest systematic uncertainties cancel in the ratio. Preliminary ALICE results are shown in fig. 4(a) for central and fig. 4(b) for peripheral events. Blue bands show a pQCD prediction of the contribution from prompt direct photons<sup>11–13</sup>. ALICE finds no excess of direct photons in peripheral events as data agree with pQCD predictions within the uncertainties. In central collisions, the direct photon yield agrees with the prompt photon yield at high  $p_T$  but indicate additional excess at low  $p_T$ .

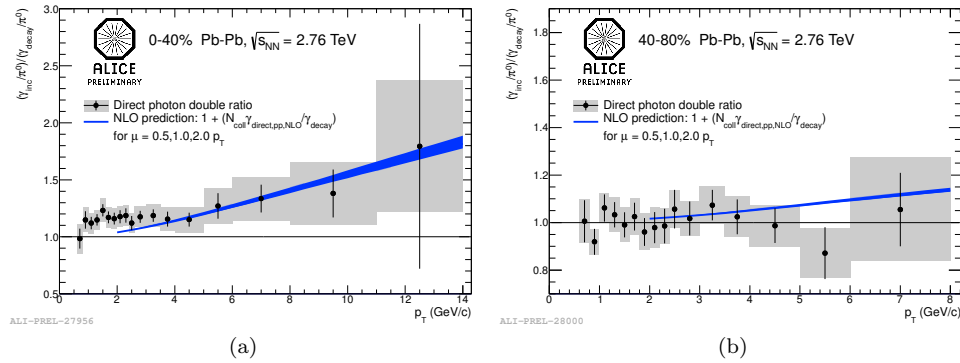


Fig. 4. Photon double ratios in central (a) and peripheral (b) Pb-Pb collisions at  $\sqrt{s_{NN}} = 2.76$  TeV.

From the measured double ratio (fig. 4), the direct photon spectrum is derived as  $N_\gamma^{dir} = (1 - 1/R_\gamma)N_\gamma^{inclusive}$  and plotted in fig. 5. For comparison, pQCD predictions<sup>12,13</sup> are shown by the blue band. In addition, in the region  $p_T < 2$  GeV/c where one expects a dominant contribution of thermal direct photons, ALICE fit the data and extracted the inverse slope. However, one should keep in mind that this slope is influenced by collective expansion and the entire evolution of the system and therefore should not be directly interpreted as the temperature in the center of the fireball.

The collective flow of direct photons is extremely interesting because it is expected that direct photons are emitted from the hottest stage of the collision and

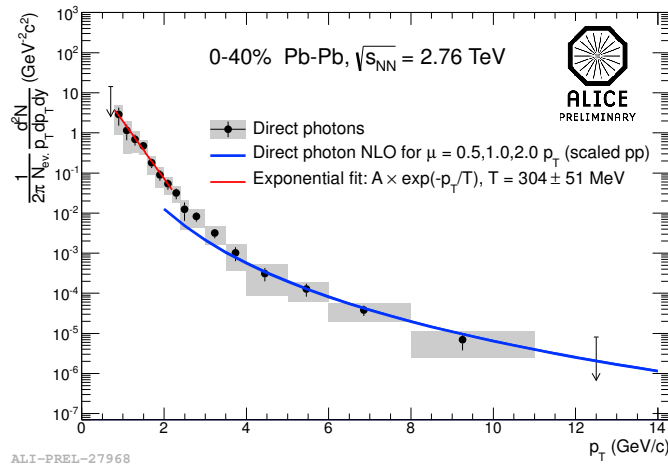


Fig. 5. Direct photon spectrum in central (0-40%) Pb-Pb collisions at  $\sqrt{s_{NN}} = 2.76$  TeV. The blue line represents pQCD prompt photon predictions while the red line is an exponential fit in the range  $0.9 < p_T < 2.0$  GeV/c.

their flow reflects the development of collective expansion at early stages. Experimentally, one can measure the flow of inclusive photons, estimate the flow of decay photons and estimate the flow of direct photons as

$$v_n^{\gamma,dir} = \frac{v_n^{\gamma,incl} R_\gamma - v_n^{\gamma,dec}}{1 - R_\gamma}, \quad (3)$$

where  $v_n^{\gamma,dir}$ ,  $v_n^{\gamma,incl}$  and  $v_n^{\gamma,dec}$  are the flow of direct, inclusive and decay photons with respect to the  $n^{\text{th}}$  harmonic. As one can see from equation 3, with  $R_\gamma$  close to unity, the uncertainties rapidly increase. Therefore, we present the results of direct photon flow as a comparison of collective flow of inclusive and decay photons, see figs. 6 and 7 for elliptic and triangular flow respectively. In fig. 6a (7a) the elliptic (triangular) flow contribution from inclusive photons is shown in red while the decay photons are shown in black. Predictions are also shown for Next-to-Leading-Order (NLO) prompt photons plus decay photons (blue dash-dotted line)<sup>11</sup> as well as two models for inclusive photons (decay + prompt + thermal) in the red<sup>14</sup> and green<sup>15</sup> curves. Quantitative comparisons are shown in the right insets of these figures as well. The differences are shown in units of the sigma of the total uncertainties. We found that both elliptic and triangular flow of inclusive photons are considerably smaller than the expected flow of decay photons and agree with predictions of both models incorporating thermal photon contributions.

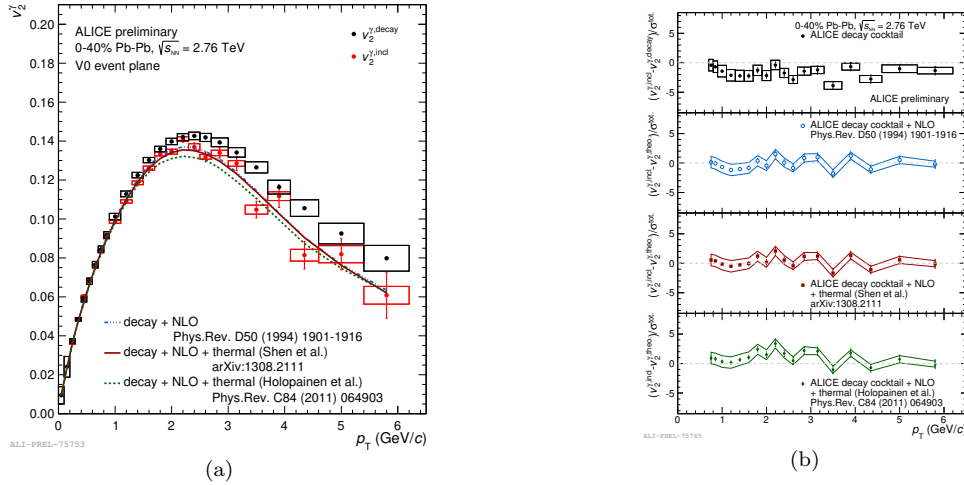


Fig. 6. (a) Comparison of elliptic flow of inclusive and decay photons. Lines represent contributions of decay photons with theoretical calculations<sup>11,14,15</sup>. (b) Difference between inclusive and decay (top plot) and inclusive and theory (3 bottom plots) elliptic flows in units of total error.

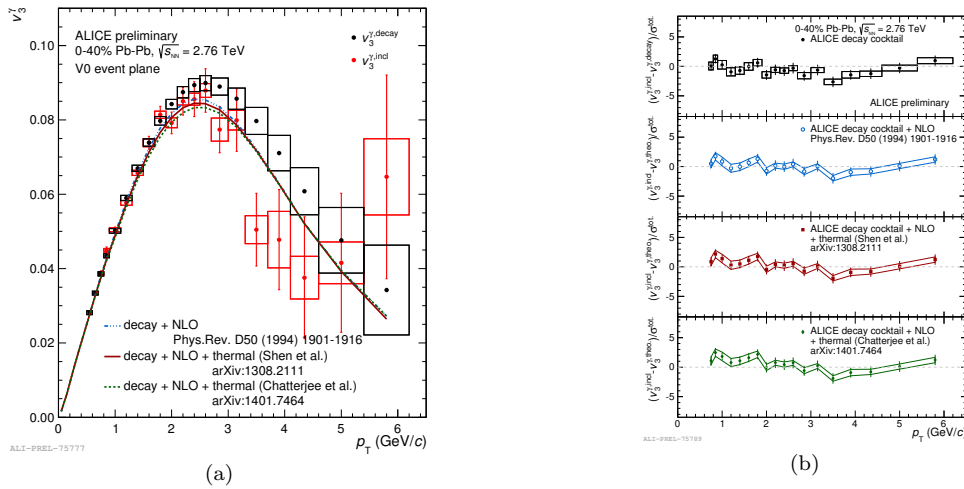


Fig. 7. Same as fig. 6 but for triangular flow.

## 5. Conclusions

We reviewed the ALICE results on production of neutral pions in pp collisions at  $\sqrt{s} = 0.9, 2.76$  and 7 TeV and neutral pions and direct photons in Pb-Pb collisions at  $\sqrt{s_{NN}} = 2.76$  TeV. QCD calculations reproduce the neutral pion spectra in pp collisions at  $\sqrt{s} = 0.9$  TeV but overpredict the pion yields at higher energies. In Pb-Pb collisions, neutral pion yields demonstrate a suppression of a factor of 10 in the most central collisions with respect to scaled pp collisions at the same energy. The

direct photon spectrum agrees with pQCD predictions at  $p_T > 4$  GeV/ $c$  but shows excess at lower  $p_T$ . Collective flow of inclusive photons differs from estimates of collective flow of decay photons and agrees with expectations including contributions from thermal photons.

### Acknowledgments

This work was partially supported by the grant RFBR 12-02-91527.

### References

1. K. Aamodt *et al.*, The ALICE experiment at the CERN LHC, *JINST* **3**, p. S08002 (2008).
2. B. B. Abelev *et al.*, Neutral pion production at midrapidity in pp and Pb-Pb collisions at  $\sqrt{s_{NN}} = 2.76$  TeV, *Eur.Phys.J.* **C74**, p. 3108 (2014).
3. B. Abelev *et al.*, Neutral pion and  $\eta$  meson production in proton-proton collisions at  $\sqrt{s} = 0.9$  TeV and  $\sqrt{s} = 7$  TeV, *Phys.Lett.* **B717**, 162 (2012).
4. D. d'Enterria, K. J. Eskola, I. Helenius and H. Paukkunen, LHC data challenges the contemporary parton-to-hadron fragmentation functions, *PoS DIS2014*, p. 148 (2014).
5. G. Aad *et al.*, Measurement of inclusive jet and dijet production in *pp* collisions at  $\sqrt{s} = 7$  TeV using the ATLAS detector, *Phys.Rev.* **D86**, p. 014022 (2012).
6. D. de Florian, R. Sassot, M. Epele, R. J. Hernandez-Pinto and M. Stratmann, Parton-to-Pion Fragmentation Reloaded, arXiv:1410.6027 (2014).
7. S. Adler *et al.*, A Detailed Study of High-p(T) Neutral Pion Suppression and Azimuthal Anisotropy in Au+Au Collisions at  $\sqrt{s_{NN}} = 200$  GeV, *Phys.Rev.* **C76**, p. 034904 (2007).
8. R. Sharma, I. Vitev and B.-W. Zhang, Light-cone wave function approach to open heavy flavor dynamics in QCD matter, *Phys.Rev.* **C80**, p. 054902 (2009).
9. R. Neufeld, I. Vitev and B.-W. Zhang, A possible determination of the quark radiation length in cold nuclear matter, *Phys.Lett.* **B704**, 590 (2011).
10. W. Horowitz and M. Gyulassy, The Surprising Transparency of the sQGP at LHC, *Nucl.Phys.* **A872**, 265 (2011).
11. L. Gordon and W. Vogelsang, Polarized and unpolarized isolated prompt photon production beyond the leading order, *Phys.Rev.* **D50**, 1901 (1994).
12. W. Vogelsang and M. R. Whalley, A compilation of data on single and double prompt photon production in hadron hadron interactions, *J. Phys.* **G23**, A1 (1997).
13. W. Vogelsang. Private communications (August, 2004).
14. C. Shen, U. W. Heinz, J.-F. Paquet, I. Kozlov and C. Gale, Anisotropic flow of thermal photons as a quark-gluon plasma viscometer, arXiv:1308.2111 (2013).
15. H. Holopainen, S. Rasanen and K. J. Eskola, Elliptic flow of thermal photons in heavy-ion collisions at Relativistic Heavy Ion Collider and Large Hadron Collider, *Phys.Rev.* **C84**, p. 064903 (2011).